ChemComm

COMMUNICATION

Solvent-assisted mechanochemical crystallization of metal-free perovskite solid solution (H_2dabco, H_2hmta)$NH_4(BF_4)_3$

Received 00th January 20xx,
Accepted 00th January 20xx

DOI: 10.1039/x0xx00000x

Jumpei Moriguchi, [a] Tomoe Koga, [b] Nao Tsunoji, [c] Sadafumi Nishihara, [c] Tomoyuki Akutagawa, [d] Atsuko Masuya-Suzuki [a,b] and Ryo Tsunashima *[a,b]

All-proportional solid solutions of the metal-free perovskite (H_2dabco$_{1-y}$, H_2hmta$_y$)$(NH_4)(BF_4)_3$ ((d,h)-BF_4) were crystallized via a mechanochemical method. Their molecular dynamics depend on ratio *y* with a compositional boundary at *y* = 0.43, where H_2dabco^{2+} was deduced to be at a dynamic disorder state, even below phase transition temperature to plastic crystalline phase seen at *y* = 0.

Perovskite-type oxides in functional materials such as ferroelectrics and piezoelectrics are often found in solid solution.[1,2] This is because their chemical and physical properties can be finely controlled by a combination and ratio of metal ions. A solid solution with different structural symmetries also exhibits unique physical properties related to structural instability at the compositional boundary of components, known as a morphotropic phase boundary, such as lead zirconate titanate.[3–5]

In 2002 the third type of ABX_3 perovskite structures was reported, followed by traditional fully inorganic perovskite and organic-inorganic hybrid perovskite.[6] Both A-sites and B-sites are occupied by molecular ions instead of metal, in what are known as the metal-free molecular perovskites. In 2018 ferroelectricity was realized using non-centrosymmetric organic molecules at the A-site.[7] Successive reports have described properties of these materials, including visible luminescence with high fluorescence quantum yields, and X-ray detection.[8–12] These materials have advantageous qualities with respect to reduced effects on humans and the environment more broadly. Spontaneous polarization of perovskites is often caused by distortion of $\{BX_6\}$ octahedron. Unlike metal-containing systems however, whose distortion usually originates from metal ions via the pseudo-Jahn-Teller effect, the $\{(NH_4)X_6\}$ octahedron in metal-free perovskite does not have a mechanism for spontaneous polarization. Both polarization and dielectric properties are affected by characteristics of interaction, steric hindrances, symmetry, and orientation of the A-site molecule.

We have investigated solid solutions of A-site molecules with different characteristics; hexamethylenetetramine (hmta) and 1,4-diazabicyclo[2.2.2]octane (dabco). In the perovskite structure, non-centrosymmetric $(H_2hmta)(NH_4)Br_3$ (**h-Br**)[13] was mixed with centrosymmetric $(H_2dabco)(NH_4)Br_3$ (**d-Br**), resulting in the solid solution (H_2dabco,H_2hmta)$(NH_4)Br_3$ (**(d,h)-Br**). Unlike **d-Br**, which underwent first-order type phase transition to plastic crystalline (PC) phase at 327 K,[7] second-order type transition with Debye-type dielectric relaxation at approximately 200 K was observed for **(d,h)-Br**. It was considered that H_2hmta^{2+} induced structural fluctuations in the lattice that activates the thermal motion of surrounding H_2dabco^{2+}.[14] However, the solid solution was crystallized from an aqueous solution, and hmta was only miscible below a few mol% due to hydrolysis in the acidified aqueous solution.

Mechanochemical methods[15–22] are techniques for reacting components via mechanical processes such as compression and shearing. This can facilitate products and reactions that differ from those associated with solution-based synthesis.[15–17] Metal-free perovskites have been crystallized via mechanochemical methods.[18] Additionally, mechanochemical methods have been used to achieve solid solutions of species that are difficult to mix in solution or the liquid phase.[19–22]

The present study investigated the use of mechanochemical methods to crystallize solid solutions of the metal-free perovskite crystals between $(H_2hmta)(NH_4)(BF_4)_3$ (**h-BF_4**) and $(H_2dabco)(NH_4)(BF_4)_3$ (**d-BF_4**). **d-BF_4** was reported by Fu et al.[23, 24], and undergoes phase transitions from the order phase of space group *Pa*-3 (phase III) to PC phase (phase II; *Fm*-3c) at 333 K, losing the orientational order of H_2dabco^{2+}. The hmta analogue **h-BF_4** was newly crystallized in the current study, and underwent transition to phase II at 390 K from tetragonal phase (phase IV; $I4_1/a$).[‡] We successfully crystallized **((d,h)-BF_4)** with a wide range of compositions, and compositional dependence of phase transition behaviour was investigated.

[a] Graduate School of Sciences and Technology for Innovation, Yamaguchi University, Yoshida 1677-1, Yamaguchi, 753-8512, Japan.
[b] Chemistry Course, Faculty of Science, Yamaguchi University, Yoshida 1677-1, Yamaguchi,753-8512, Japan.
[c] Graduate School of Advanced Science and Engineering, Hiroshima University, Higashi-Hiroshima 739-8526, Japan.
[d] Institute of Multidisciplinary Research for Advanced Materials (IMRAM), Tohoku University, Sendai 980-8577, Japan.

† Electronic Supplementary Information (ESI) available. Method, FT-IR spectra, TG-DTA, LC-MS, DSC, powder X-ray diffraction, complex permittivity, solid-state ^{13}C-NMR. CCDC 2347881, 2347882. For ESI and crystallographic data in CIF or another electronic format See DOI: 10.1039/x0xx00000x

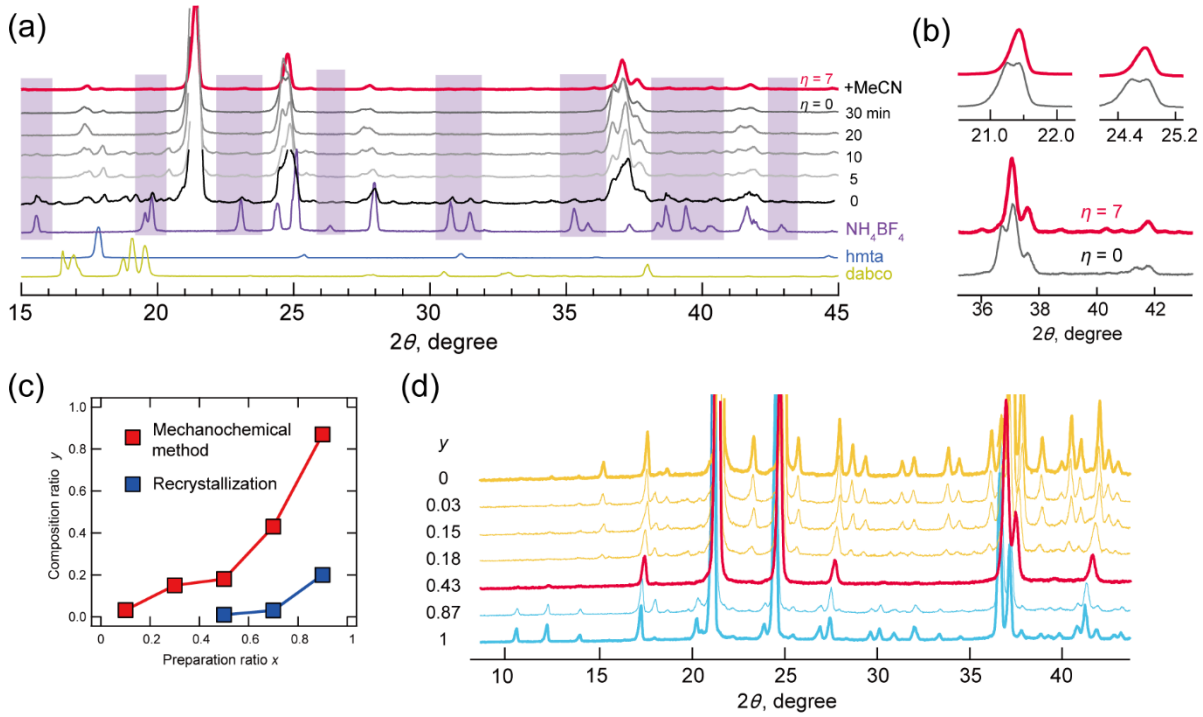

Figure 1. (a) Time evolution of P-XRD patterns of solids mixed after grinding for 0, 5, 10, 20 and 30 minutes, and P-XRD pattern of the solid solution prepared by grinding with the addition of acetonitrile for 30 min (black). (b) Extended graph of the P-XRD patterns of η = 0 and 7. (c) Plots of mixing ratio x and composition ratio y for mechanochemical (red) and recrystallization (blue) methods. (d) P-XRD patterns of solid solution prepared via mechanochemical methods at variable y.

The powder X-ray diffraction (P-XRD) patterns of a mixture of dabco (5.0 mmol), hmta (5.0 mmol), NH_4BF_4 (7.5 mmol), and an aqueous solution of HBF_4 (20.0 mmol) after grinding for 0, 5, 10, 20 and 30 minutes are shown in Figure 1a. At t = 0, diffractions by perovskite structure was observed in those of NH_4BF_4.With grinding a mixture diffractions by NH_4BF_4 disappeared at t > 20, indicating that NH_4BF_4 was converted to a perovskite structure. Some diffractions were split however, indicating low structural purity. Mechanochemical synthesis often proceeds via the addition of solvent,[20,21, 25–27] where methods can be classified with parameter η as neat (η = 0), liquid-assisted grinding (η = 0–2 μL mg^{-1}), slurrying (η = 2–12 μL mg^{-1}), and solution (η > 12).[17] Parameter η is defined by equation 1 below, where V is the amount of solvent (μL) and m is reactant weight (mg):

$$\eta = V/m \qquad \text{eq.1}$$

In the present study split diffraction patterns at η = 0 were improved at η = 7 via the addition of acetonitrile (red line; Figure 1a and 1b). Mechanochemical reactions at η = 7 with acetonitrile were then performed with various mixing ratios (0.1, 0.3, 0.5, 0.7 and 0.9) for hmta (10x mmol), dabco (10−10x) mmol), NH_4BF_4 (10−5x mmol) and HBF_4 (20 mmol). For comparison, corresponding crystallizations were also performed by dissolving the compounds in water.

The compositions y (dabco; hmta = 1−y:y) in solid solutions were plotted for mechanochemical methods (red) and recrystallization from water (blue) (Figure 1c). These y values determined by peak area in liquid chromatography-mass spectrometry and elemental analysis were relatively concordant (calibration in Figure S3-1, experimental results in Tables S3 and S4-1). In all cases the y values obtained via mechanochemical methods were higher than those obtained via recrystallization. This is accounted for by hydrolysis of hmta by acid. Respective ratios y for mixing ratios x of 0.1, 0.3, 0.5, 0.7, and 0.9 were 0.03, 0.15, 0.18, 0.43 and 0.87. Solid solutions crystallized via mechanochemical methods were all-proportional solid solutions.

Figure 1d shows the P-XRD patterns of solid solutions prepared via mechanochemical methods, measured at room temperature. Diffraction patterns of lower hmta contents, y = 0.03, 0.15 and 0.18 (indicated by yellow lines in Figure 1d) corresponded to that of static phase **d-BF$_4$** (space group *Pa*-3, phase III). At y = 0.43 the diffraction pattern (indicated by a red line) differed from **d-BF$_4$** and **h-BF$_4$** above 93 K (Figure S4-1). This corresponds well with that of their PC phase (phase II, comparisons are shown in Figure S4-1). At y = 0.87 the diffraction pattern was consistent with that of the static phase of **h-BF$_4$** (phase IV). These experimental results indicated compositional phase transition in between **d-BF$_4$** and **h-BF$_4$**, where anomaly phase (phase V) appeared at their boundary y = 0.43.

Lattice parameters of solid solutions were evaluated, and composition dependence of lattice length and volume normalized for ABX_3 composition are shown in Figures 2a and 2b. The lattice dimensions were linearly associated with composition. This is a typical relationship in all-proportional solid solutions, known as Vegard's law.

Respective transition temperatures of **d-BF$_4$** and **h-BF$_4$** to PC phase were 332 K and 392 K. Differences in intermolecular

interactions, and high symmetry of hmta contribute to higher transition temperatures. Solid state hmta melted at 536 K without transition to PC phase, even though dabco transitioned to PC phase at 351 K before melting (434 K). This is considered to be because highly symmetrical hmta has a lower entropy change with respect to transition.[28] Results of differential thermal analysis (DTA) and differential scanning calorimetry (DSC) are summarized in Table S4-2, Figure S4-2 and Figure S4-3. Thermal anomaly which indicates transition to phase II (transition temperature T_2) were observed except for the case y = 0.43. At approximately 450 K (transition temperature T_1) thermal anomaly was also observed for y = 0, 0.03, 0.15, 0.18 and 0.43 in the DTA chart. This is considered to represent disordering of BF_4^- (phase I). Phase transition enthalpy against y is shown in Figure 2c, and a phase diagram is shown in Figure 2d. Transition enthalpies and temperature decreased toward y = 0.43, at which point thermal anomaly disappeared in both DSC and DTA.

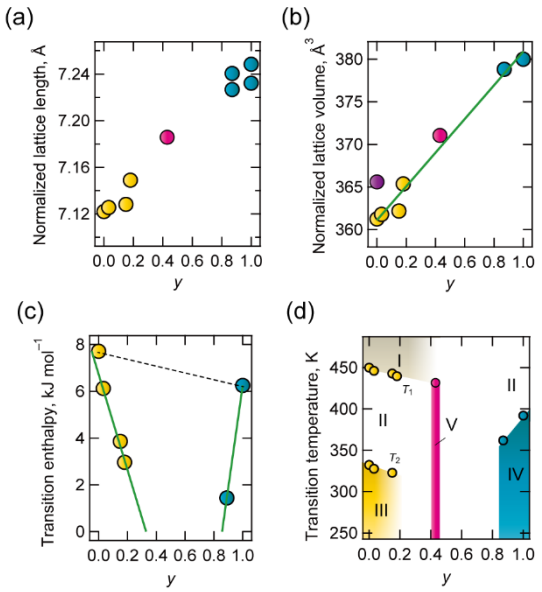

Figure 2. Component dependence of (a) normalized lattice length, (b) normalized lattice volume (purple circle represents values at phase II of d-BF4), (c) transition enthalpy to phase II from phase III (yellow) or phase IV (blue) and (d) phase diagram.

At the transition from ordered phase III or IV to disordered phase II, the compositional average of enthalpy change, $\Delta H(y)$, is represented by

$$\Delta H(y) = (1-y)\Delta H\ (\mathbf{d\text{-}BF_4}) + y\Delta H\ (\mathbf{h\text{-}BF_4}) \qquad \text{eq.2}$$

with ΔH (**d-BF$_4$**) (7.71 kJ mol^{-1}) and ΔH (**h-BF$_4$**) (6.11 kJ mol^{-1}). This model assumes that H_2hmta^{2+} and H_2dabco^{2+} are independently behave at phase transitions. However, experimental values do not follow this model (dotted line in Figure 2c), indicating that H_2hmta^{2+} and H_2dabco^{2+} are randomly distributed in the solid state, and the thermal motion of each is correlated. We consider that the structural correlation may be due to a structural relationship between A-site molecule and $\{NH_4(BF_4)_6\}$ octahedron.

Lattice length and volume were consistent with the compositional average, but their phase transition behaviours were not. In addition, the compositional boundary was observed at y = 0.43, where (i) the diffraction pattern was consistent with that of the PC phase of cubic *Fm*-3*c* above 223 K, but (ii) thermal anomaly identical to first-order-type phase transition disappeared. Unit cell volume normalised for composition was 371 Å^3 for y = 0.43 at room temperature, which is larger than the 367 Å^3 of phase II of **d-BF$_4$**, but smaller than the 395 Å^3 of **h-BF$_4$**. H_2dabco^{2+} molecules at y = 0.43 are thus considered to be in enough space to exhibit rotational disorder, but hmtaH_2^{2+} is not. One possible structure proposed at y = 0.43 at approximately room temperature is a mixture of static (random) orientational disorder of H_2hmta^{2+} and dynamic disorder of H_2dabco^{2+}. Solid-state ^{13}C-NMR (NMR = nuclear magnetic resonance; Figure S4-9) was characterized for y = 0.43, **d-BF$_4$** and **h-BF$_4$** at 300 K, and results are summarized in Table S4-1. Peaks for dabco and hmta at y = 0.43 were sharper than those associated with **d-BF$_4$** and **h-BF$_4$**. This implies that A-site molecules at y = 0.43 are in higher structural symmetry. This is consistent with our structural model.

The dynamics of molecular motion were investigated via temperature variable complex permittivity measurements. Solid solution **(d,h)-BF$_4$** (y = 0.03, 0.15, 0.18, 0.43 and 0.87) exhibited identical frequency and temperature dispersion at 100–300 K (Figure S4-4 to S4-8) due to Debye-type electric dipole relaxation. Corresponding anomaly was not observed for **d-BF$_4$**, but was observed for **h-BF$_4$** at different temperature ranges above 300 K. A plot of activation energy and temperatures at 0.01 Hz estimated from the Arrhenius relationship is shown in Figure 3a. These values were less dependent on composition at 0.3-0.4 eV and ~130 K respectively, indicating that the dipole relaxations have same origin. In contrast, ε_1, ε_2 and D ($\equiv \varepsilon_2/\varepsilon_1$) values strongly depend on y. D values at 1 MHz at different y points are shown in Figure 3b. Peak top temperature did not depend on y, but the peak was largest at y = 0.43. We consider that this dipole relaxation originated from thermal motion of the H_2dabco^{2+} and/or $\{NH_4(BF_4)_6\}$ octahedron, whose static order melt point is approximately 140 K.

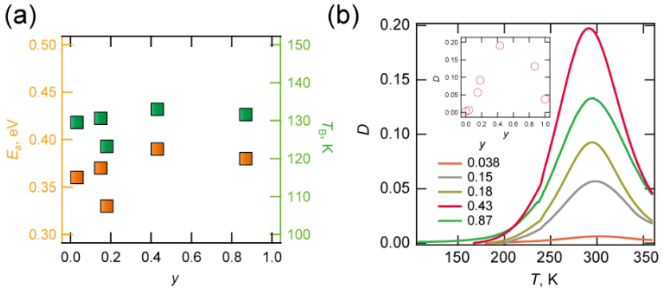

Figure 3. (a) Plot of activation energy E_a and temperature T_B estimated for f = 0.01 Hz via Arrhenius plotting, and (b) plot of D against T at variable y (inset; plot of D at 300 K with y).

In summary, mechanical methods crystallized all-proportional solid solutions of **d-BF$_4$** and **h-BF$_4$**. Even though lattice dimensions were proportional to y, thermodynamic values of phase transition were not. As y increased, unit cell

volume exceeded that of PC phase **d-BF_4**, and the compositional boundary appeared at y = 0.43, where high symmetric cubic-type diffraction was observed above 223 K. We considered the structural mode of the boundary to be a random mixture of thermally dynamic H_2dabco^{2+} and orientationally disordered H_2hmta^{2+}. Phase transition temperature and molecular dynamics strongly depend on the ratio of the two, clearly indicating that solid metal-free perovskite solution is advanced and effective for tuning physical properties, as are traditional perovskites, where mechanical crystallization is a useful technique for all-proportional solid solution. We think that band tuning for optoelectronic properties is also possible, because A-site molecules contributed to the electronic state (band gap) of the crystal.[29]

The authors acknowledge the extensive contribution of Structural Sciences from Leading-Edge Materials to Cultural and Archaeological Works, Yamaguchi University. We also express our gratitude to Mr. Matsuoka, Institute of Systems Biology and Radioisotope Analysis, Yamaguchi University, for his valuable advice and support with the analysis of liquid chromatography-mass spectrometry conducted using Thermo Fisher Orbitrap Exploris 120.

Conflicts of interest

There are no conflicts to declare.

Data availability

†The data supporting this article have been included as part of the ESI.

Notes and references

‡**h-BF_4** was isolated as colourless block single crystals from mixed aqueous hmta and HBF_4 solution (Figure S2-1). Details on the crystallization procedure and characterization are included in the Electronic Supplementary Information. In temperature-variable single crystal X-ray diffraction studies (Table S1 and Figures S2-3 and S2-4) and thermal DTA (Figure S2-5) and DSC (Figure S2-6) analyses, phase transition from space group $I4_1/a$ (ordered phase) to *Fm*-3*c* (PC disordered phase) where A-site molecule was disordered but the orientation of BF_4^- was frozen, was observed at 392 K. In temperature and frequency dependence measurements of complex permittivity, Debye-type relaxation was observed above 300 K (Figure S2-7). Activation energy for dipole relaxation was estimated to be 0.78 eV, based on an Arrhenius plot (Figure S2-8). We consider that this originates from thermal disorder of H_2hmta^{2+} toward transition to PC phase.

1 I. Grinberg, D. V. West, M. Torres, G. Gou, D. M. Stein, L. Wu, G. Chen, E. M. Gallo, A. R. Akbashev, P. K. Davies, J. E. Spanier and A. M. Rappe, *Nature*, 2013, **503**, 509-512.
2 X. Hou and J. Yu, *J. Am. Ceram. Soc.*, 2013, **96**, 2218-2224.
3 B. Jaffe, R. S. Roth and S. Marzullo, *J. Appl. Phys*., 1954, **25**, 809-810.
4 Z. H. Liu, A. R. Paterson, H. Wu, P. Gao, W. Ren and Z. G. Ye, *J. Mater. Chem. C*, 2017, **5**, 3916-3923.
5 W. Q. Liao, D. Zhao, Y. Y. Tang, Y. Zhang, P. F. Li, P. P. Shi, X. G. Chen, Y. M. You and R. G. Xiong, *Science,* 2019, **363**, 1206-1210.
6 C. A. Bremner, M. Simpson and W. T. A. Harrison, *J. Am. Chem. Soc*., 2002, **124**, 10960-10961.
7 H. Y. Ye, Y. Y. Tang, P. F. Li, W. Q. Liao, J. X. Gao, X. N. Hua, H. Cai, P. P. Shi, Y. M. You and R. G. Xiong, *Science*, 2018, **361**, 151-155.
8 X. Song, Q. Li, J. Han, C. Ma, Z. Xu, H. Li, P. Wang, Z. Yang, Q. Cui, L. Gao, Z. Quan, S. F. Liu and K. Zhao, *Adv. Mater*., 2021, **33**, e2102190.
9 H. S. Wu, B. T. Murti, J. Singh, P. K. Yang and M. L. Tsai, *Adv. Sci*., 2022, **9**, 2104703.
10 X. Song, G. Hodes, K. Zhao and S. F. Liu, *Adv. Energy Mater*., 2021, **11**, 2003331.
11 Z. Z. Li, G. Q. Peng, Z. H. Li, Y. K. Xu, T. Wang, H. X. Wang, Z. T. Liu, G. Wang, L. M. Ding and Z. W. Jin, *Angew. Chem. Int. Ed*., 2023, **62**, e202218349.
12 X. Song, T. Li, H. Li, S. Lin, J. Yin and K. Zhao, *Sci. China Mater.*, 2024, **67**, 1348-1355.
13 H. Morita, R. Tsunashima, S. Nishihara, K. Inoue, Y. Omura, Y. Suzuki, J. Kawamata, N. Hoshino and T. Akutagawa, *Angew. Chem. Int. Ed*., 2019, **58**, 9184-9187.
14 H. Morita, R. Tsunashima, S. Nishihara and T. Akutagawa, *CrystEngComm*, 2020, **22**, 2279-2282.
15 T. Seo, N. Toyoshima, K. Kubota and H. Ito, *J. Am. Chem. Soc*., 2021, **143**, 6165-6175.
16 G. W. Wang, K. Komatsu, Y. Murata and M. Shiro, *Nature*, 1997, **387**, 583-586.
17 T. Friščić, C. Mottillo and H. M. Titi, *Angew. Chem*., 2020, **132**, 1030-1041.
18 F. Lyu, Z. Chen, R. Shi, J. Yu and B. L. Lin, *J. Solid State Chem.*, 2021, **304**, 122548.
19 A. Karmakar, A. M. Askar, G. M. Bernard, V. V. Terskikh, M. Ha, S. Patel, K. Shankar and V. K. Michaelis, *Chem. Mater.*, 2018, **30**, 2309-2321.
20 M. Lusi, I. J. Vitorica-Yrezabal and M. J. Zaworotko, *Cryst. Growth Des*., 2015, **15**, 4098-4103.
21 E. Batisai, M. Lusi, T. Jacobs and L. J. Barbour, *Chem. Commun.*, 2012, **48**, 12171-12173.
22 R. Tsunashima, *CrystEngComm*, 2022, **24**, 1309-1318.
23 G. Z. Liu, J. Zhang and L.-Y. Wang, Synth. React. Inorg., Met.-Org., Nano-Met. Chem., 2011, **41**, 1091-1094.
24 L. L. Chu, T. Zhang, W. Y. Zhang, P. P. Shi, J. X. Gao, Q. Ye and D. W. Fu, *J. Phys. Chem. Lett*. 2020, **11**, 1668-1674.
25 E. Schur, E. Nauha, M. Lusi and J. Bernstein, *Chemistry*, 2015, **21**, 1735-1742.
26 B. Saikia, A. Seidel-Morgenstern and H. Lorenz, *Cryst. Growth Des*., 2021, **21**, 5854-5861
27 D. Braga, L. Maini and F. Grepioni, *Chem. Soc. Rev*., 2013, **42**, 7638-7648.
28 L. N. Becka and D. W. J. Cruickshank, *Proc. R. Soc. Lond. A. Math. Phys. Sci.* 1963, **273**, 435-454.
29 J. Bie, D. B. Yang, M. G. Ju, Q. Pan, Y. M. You, W. Fa, X. C. Zeng and S. Chen, *JACS Au*, 2021, **1**, 475-483.

